An accuracy analysis of the front tracking method and interface capturing methods for the solution of heat transfer problems with phase changes

Lubomír Klimeš, Tomáš Mauder, Pavel Charvát, Josef Štětina

Brno University of Technology, Energy Institute, Department of Thermodynamics and Environmental Engineering, Technická 2896/2, 616 69 Brno, Czech Republic

E-mail: klimes@fme.vutbr.cz

Abstract. Materials undergoing a phase change have a number of applications in practice and engineering. Computer simulation tools are often used for investigation of such heat transfer problems with phase changes since they are fast and relatively not expensive. However, a crucial issue is the accuracy of these simulation tools. Numerical methods from the interface capturing category are frequently applied. Such approaches, however, allow for only approximate tracking of the interface between the phases. The paper presents an accuracy analysis and comparison of two widely used interface capturing methods—the enthalpy and the effective heat capacity methods—with the front tracking algorithm. A paraffin-based phase change material is assumed in the study. Computational results show that the front tracking algorithm provides a significantly higher accuracy level than the considered interface capturing methods.

1. Introduction

Phase change materials (PCMs) and latent heat thermal energy storage (LHTES) have recently attracted attention of many researchers. Applications of PCM and LHTES include, e.g. air heating systems [1], thermal energy storage [2], air conditioning [3] and stabilization of temperature [4]. As experimental investigations are usually expensive and time consuming, most researchers tend to utilize computer simulation tools. Such tools allow for relatively inexpensive simulations, analyses and optimization. The high computing speed and the high computational accuracy are required, although these requirements are usually opposite to each other.

A computer simulation of PCMs and LHTES involves the solution of a heat transfer problem with the phase change. In general, there are two main categories of numerical methods for this purpose: interface/front capturing methods and interface/front tracking methods [5]. Interface capturing (latent heat evolution) methods are easy for implementation but almost no effort is devoted to the precise determination of the front location. Typical methods from the interface capturing category are the well-known enthalpy method [6] and the effective heat capacity method [7]. On the other hand, though the interface tracking methods are significantly more difficult from the mathematical, programming as well as computational point of view, they offer a more precise determination of the front location and of the temperature distribution. The fulfilment of the energy conservation is accurate since the energy balance at the interface is handled explicitly as a kind of the boundary condition. Shyy *et al.* [8] presented a comprehensive overview of the front tracking algorithms for computational fluid dynamics problems including

moving boundaries. Udaykumar *et al.* [9] proposed a front tracking algorithm based on mixed Lagrangian-Eulerian approach. The interface was tracked explicitly with the Lagrangian approach but the heat transfer equation was solved on a fixed grid in the Eulerian manner. Li *et al.* [10] presented a front tracking algorithm with the heat diffusion (conduction) as the only heat transfer mechanism. The method was validated with the use of exact analytical solutions and the authors concluded that the method is of a high accuracy. Browne et al. [11] applied the front tracking method for the simulation of the grain growth in a solidifying alloy. The method was used for the analysis of both the columnar and equiaxed grain zones. Recently, Seredynski *et al.* [12] presented the front tracking method for modelling of a binary alloy solidification and a solid-liquid phase transition of semi-transparent material. The front tracking algorithm was used for the prediction of the macro-segregation and a numerical method for investigation of phase change processes in semi-transparent materials was developed. McFadden and Browne [13] used the front tracking method for the macro-structure prediction during alloy solidification. The developed model utilizes the Schneil equation for the description of the non-linear latent heat evolution and a log-normal distribution is applied to model the activation of nuclei. Banaszek and Seredynski [14] applied the front tracking method for identification of distinct dendritic regions, which are present in the mushy zone during the solidification of binary alloys. The authors concluded that the solid volume fraction, which is used to distinguish the distinct regions, is not constant and it is a function of time and location with respect to the phase interface.

In the paper, we present an accuracy analysis and comparison of the front tracking method and two interface capturing methods—the enthalpy method and the effective heat capacity method. The front tracking method described by Li *et al.* [10] is adopted and the Stefan problem with an isothermal phase change is considered. We deal with a 1D case which allows us to employ the exact solution to the Stefan problem for validation of the results. The comparison of results and the accuracy analysis show that the front tracking algorithm allows for simulations with a significantly higher accuracy level than in case of the considered interface capturing methods.

2. Interface capturing and interface tracking methods for Stefan problems

A brief description of the considered interface tracking and interface capturing methods follows.

2.1. Enthalpy method

In general, the spatially- and time-dependent temperature distribution of the matter is a solution to the transient heat transfer problem, which can be mathematically modelled by the governing equation

$$\varrho c_p \frac{\partial T}{\partial t} = \operatorname{div}\left(k \nabla T\right) + \dot{g} \tag{1}$$

where T is the temperature, t is time, ϱ stands for the density, c_p is the specific heat at constant pressure, k is the thermal conductivity and $\dot{g}$ represents an internal source of heat. In case of the Stefan problem with the phase change, a crucial task is to determine the term $\dot{g}$, which accounts for the latent heat of phase change.

In the enthalpy method, a new thermodynamic variable—the enthalpy—is introduced to incorporate the latent heat and the sensible heat together. The enthalpy as a function of the temperature is defined [6] as

$$H(T) = \int_0^T \left(\varrho c_p - \varrho L_\mathrm{f} \frac{\partial f_\mathrm{s}}{\partial \theta} \right) \mathrm{d}\theta \tag{2}$$

where L_f is the latent heat of phase change and f_s is the solid fraction. The term $f_\mathrm{s} \in \langle 0, 1 \rangle$ is proportional the ratio between the solid and liquid phases. Since for the latent heat holds that

$$\dot{g} = \varrho c_p \frac{\partial f_\mathrm{s}}{\partial T} \frac{\partial T}{\partial t}, \tag{3}$$

the substitution of the differentiated Eq. (2) and Eq. (3) to the governing equation Eq. (1) leads to the enthalpy-formulated governing equation of the Stefan problem [6]

$$\frac{\partial H}{\partial t} = \mathrm{div}\,(k\nabla T)\,. \tag{4}$$

The governing Eq. (4) now contains two unknown variables–the enthalpy and temperature–which are coupled together. This means that the enthalpy method requires a two-step solution procedure. First, the enthalpy is determined and then, in the second step, the temperature is calculated from the known enthalpy-temperature relationship. A typical dependence of the enthalpy on the temperature for a non-isothermal phase change is shown in Figure 1. The material considered in Figure 1 undergoes the phase change in the temperature interval between $T_m - \Delta T$ and $T_m + \Delta T$. Obviously, $\Delta T \to 0$ is required in case of the isothermal phase change. However, this treatment leads to numerical difficulties. The reason is that the enthalpy is no longer the function from the mathematical point of view for $\Delta T \to 0$. Instead, there is no unique mapping between the phase change temperature T_m and the enthalpy. A common practice is therefore to set $\Delta T > 0$ sufficiently small for an approximation of the isothermal phase change.

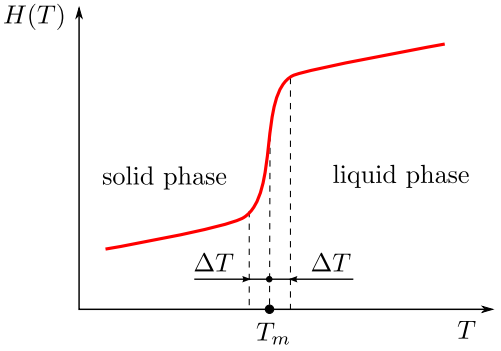

Figure 1. A typical enthalpy-temperature dependence.

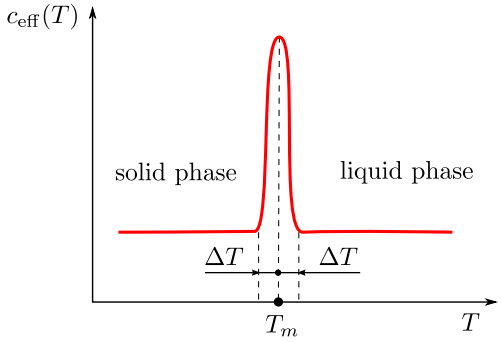

Figure 2. A characteristic temperature-dependent effective heat capacity.

2.2. Effective heat capacity method

A similar approach as in case of the enthalpy method is employed in the effective heat capacity method. Here, the latent heat is incorporated to the specific heat of the material, which is also called the heat capacity [7]. Such heat capacity is called the effective heat capacity c_{eff}, often also the apparent heat capacity. This approach leads to the artificial increase of the actual specific heat in the temperature range where the phase change takes place. A typical temperature-dependent effective heat capacity has the form of the bell shape function as shown in Figure 2. The substitution of c_{eff} to the governing Eq. (1) leads to the effective heat capacity formulation

$$\varrho c_{\mathrm{eff}} \frac{\partial T}{\partial t} = \mathrm{div}\,(k\nabla T)\,. \tag{5}$$

An approach $\Delta T \to 0$ is used for modelling of the isothermal phase change as in case of the enthalpy method. In comparison to the enthalpy method, the temperature is the only unknown variable that needs to be determined. This feature slightly simplifies the procedure of the numerical solution and its computer implementation. It also enables a straightforward use of an implicit-time numerical scheme, which is an issue in case of the enthalpy method. On the other hand, the effective heat capacity method is fairly sensitive to the time step of the simulation. Namely, excessively long time step can cause over-leaping of the temperature interval of the phase change. In such case the energy balance is not conserved and the simulation provides incorrect results.

2.3. Front tracking method

The concept of interface tracking methods significantly differs from that of interface capturing methods. Further, we consider the front tracking method on a fixed grid, which allows for explicit tracking of the interface. The method is adopted from [10]. In contrary to interface capturing methods, the primary procedure is a precise tracking of the front location, which is followed by the solution of the temperature distribution. The front tracking algorithm consists of three main steps [10]: advection and reconstruction of the interface (tracking), the determination of the normal velocities at the front, and the solution of the governing equations. The front is represented by a mass-less markers, which are situated on grid lines of the domain. The proper junction of the markers approximates the moving interface, see Figure 3.

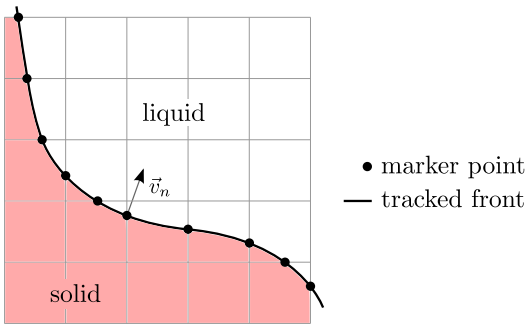

Figure 3. Front representation and marker points.

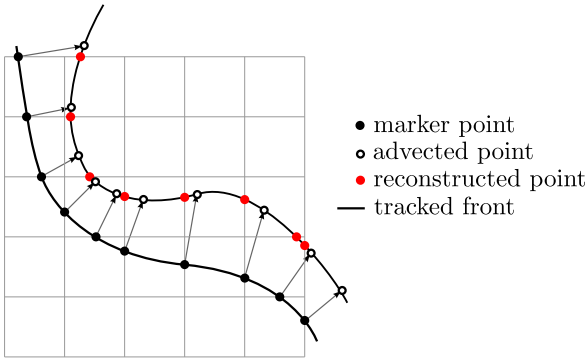

Figure 4. Advection and reconstruction of the front.

The normal vector is determined for all the markers. This direction is used for the movement of the marker with the given velocity $\vec{v}_n$. Contrary to interface capturing methods, the normal velocity of the interface is calculated explicitly with the use of the Stefan condition [15]

$$k_s \frac{\partial T_s}{\partial n} - k_\ell \frac{\partial T_\ell}{\partial n} = \varrho L_\mathrm{f} \frac{\mathrm{d}s(t)}{\mathrm{d}t} = \varrho L_\mathrm{f}\, v_n(t) \tag{6}$$

where the subscripts s and ℓ denote the solid and liquid phases, respectively, and $s(t)$ is the location of the interface as a function of time. As can be seen from Eq. (6), the Stefan condition, which expresses the energy balance at the interface, allows for the determination of the local normal velocity of the moving interface (front).

Once the normals and the normal velocities are determined, the marker points are advected within the time step Δt to new positions as shown in Figure 4. The advected points do not necessarily lie on the grid lines, and therefore the front has to be reconstructed. This includes the procedure, which locates the new marker points on the grid lines as shown in Figure 4. When the front is reconstructed, the calculation of the actual time iteration is completed with the last step: the solution of the governing equations. It has to be noted here that the governing equations are solved separately for each phase. The equations are of the form of Eq. (1) with $\dot{g} = 0$ since the latent heat is already taken into account in the Stefan condition, Eq. (6).

3. Study case: the Stefan melting problem

A one-dimensional Stefan melting problem is considered in order to compare simulation results obtained by means of the various numerical approaches. The problem is solved in a half space since an exact solution exists for this case.

The paraffin-based organic phase change material Rubitherm RT 28 HC [16] is studied. The PCM RT 28 HC has the nearly isothermal temperature T_m of the phase change, $T_m = 28\,^\circ\mathrm{C}$.

The latent heat of RT 28 HC is 215 kJ/kg, the specific heat in both the solid and liquid phases is 2 kJ/kg · K. The density of RT 28 HC is 880 kg/m^3 in the solid phase and 770 kg/m^3 in the liquid phase. The thermal conductivity is reported 0.2 W/m · K in both the phases.

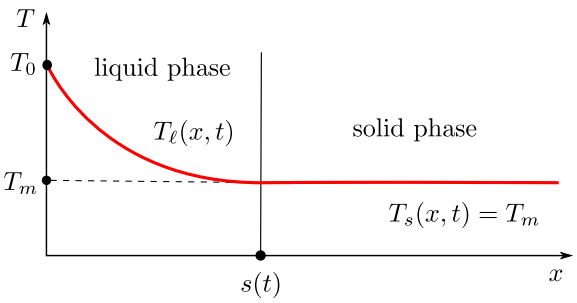

Figure 5. Schematic of the solution to the Stefan melting problem.

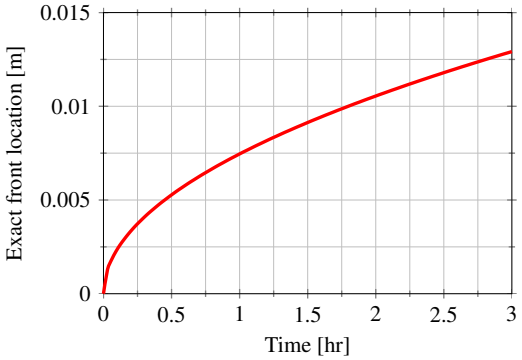

Figure 6. Exact front location.

Initially, the PCM is supposed to be in the solid phase at the melting temperature $T_m = 28\,^\circ$C. For time $t > 0$, the temperature at the boundary of the considered half space is increased to the temperature $T(x = 0, t) = T_0 = 35\,^\circ$C. Since $T_0 > T_m$, the material starts to melt from the boundary. As time goes by, the melting front propagates within the material and separates the liquid and solid phases. The melting is investigated for 3 hours from $t = 0$. The temperature distribution and the schematic of the problem is shown in Figure 5.

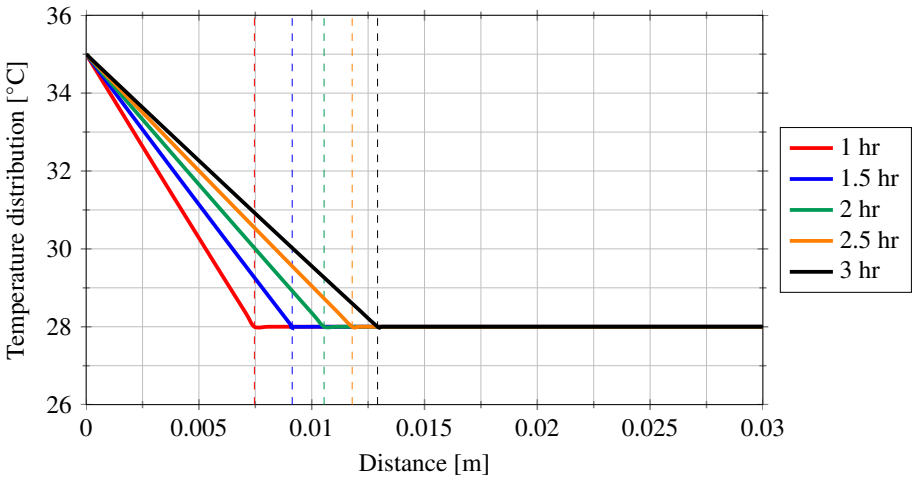

Figure 7. Exact temperature distributions and front locations.

4. Results

4.1. Exact solution to the Stefan melting problem

We employ the exact (analytical) solution, which is available to the considered Stefan melting problem in a half space. The exact solution allows us to compare the numerical (simulated) results gained with the use of distinct methods described in Section 2. Consider the Stefan melting problem described in Section 3. It can be shown that the location of the interface between the phases has the following form [15]

$$s(t) = 2\psi\sqrt{\alpha_\ell\, t} \tag{7}$$

where $\alpha_\ell = \frac{k_\ell}{\varrho_\ell c_\ell}$ is the thermal diffusivity of the liquid phase and the parameter ψ is the solution of the transcendental equation

$$\psi \, \mathrm{e}^{\psi^2} \mathrm{erf}\, \psi = \frac{c_p (T_0 - T_m)}{L_\mathrm{f} \sqrt{\pi}}. \tag{8}$$

The temperature distribution of the liquid phase is then [15]

$$T_\ell(x,t) = T_0 + \frac{(T_m - T_0)}{\mathrm{erf}\, \psi} \mathrm{erf}\left(\frac{x}{2\sqrt{\alpha_\ell t}} \right). \tag{9}$$

For the solid phase, the temperature distribution is not dependent on either the spatial variable or time and $T_s(x,t) = T_m$. The schematic of the temperature distribution within the considered half space of the Stefan melting problem is shown in Figure 5.

The exact front location given by Eq. (7) is plotted in Figure 6. Five representative and exact temperature distributions given by Eq. (9) within the PCM at time $t = 1\,\mathrm{hr}$, $t = 1.5\,\mathrm{hr}$, $t = 2\,\mathrm{hr}$, $t = 2.5\,\mathrm{hr}$ and $t = 3\,\mathrm{hr}$ are plotted in Figure 7. The actual temperature distribution within the liquid phase (see Figure 7) is fairly linear rather than exponential as plotted in Figure 5. The reason for this behaviour is a low value of the thermal conductivity and a relatively high amount of the latent heat.

4.2. Comparison of results

A series of numerical simulations was carried out for the studied case described in Section 3. The three numerical approaches described in Section 2—the front tracking method, the enthalpy method, and the effective heat capacity method—were used for simulations. The exact solution presented in Section 4.1 was used for the evaluation of the performance of numerical methods.

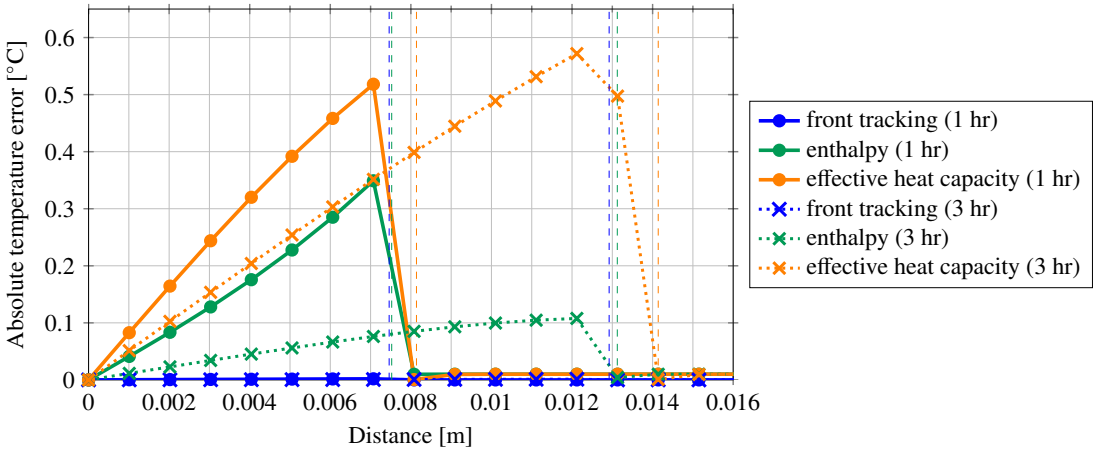

Figure 8. Absolute temperature error $|T_\mathrm{exact} - T_\mathrm{simulation}|$ at time $t = 1$ hr and $t = 3$ hr.

The simulations were run for the identical configuration of the problem. The domain with the length of 0.1 m was considered as it is a sufficient approximation of the half space for the investigated case and the simulation lasting 3 hours. The domain consisted of 101 computational nodes uniformly distributed. The spatial discretization step was therefore 1 mm. The explicit discretization scheme in time with the time step $\Delta t = 0.1\,\mathrm{s}$ was used in all the cases. Since the enthalpy and the effective heat capacity methods do not allow to simulate the isothermal phase change, the temperature range was set to a very narrow temperature interval $\langle T_m - \Delta, T_m + \Delta T \rangle$ with $\Delta T = 0.01\,^\circ\mathrm{C}$, which sufficiently approximates the isothermal phase change.

Figure 8 presents the absolute temperature error $|T_{\text{exact}} - T_{\text{simulation}}|$ at time $t = 1$ hr and $t = 3$ hr. Vertical dashed lines in Figure 8 shows the location of the front. As expected, the maximum temperature error occurs near the front location. In case of the effective heat capacity method, the local temperature error is about 0.5 °C at $t = 1$ hr and about 0.55 °C at $t = 3$ hr. For the enthalpy method, the local temperature error is smaller than in case of the effective heat capacity method. Particularly, the error is about 0.35 °C at $t = 1$ hr and about 0.1 °C at $t = 3$ hr. However, the front tracking method provides the temperature distribution with the local error, which is much smaller than in cases of the presented interface capturing methods. The local temperature error for the front tracking method is even undistinguishable in Figure 8.

Table 1. Comparison of exact and simulated results.

	Front tracking		**Enthalpy**		**Eff. heat capacity**	
	1 hr	3 hr	1 hr	3 hr	1 hr	3 hr
Maximum T error [°C]	0.001901	0.001222	0.348990	0.107770	0.518218	0.571901
Mean T error [°C]	0.000076	0.000080	0.022098	0.016667	0.030898	0.052036
Absolute $s(t)$ error [mm]	0.002137	0.002410	0.065373	0.204811	0.680325	1.220895
Relative $s(t)$ error [%]	0.0286	0.0186	0.8764	1.5853	9.1212	9.4505

Figure 9 therefore shows the detail of the temperature distribution near the front location at time $t = 1$ hr. As can be seen from the figure, the front tracking methods allows for an excelent prediction of the temperature distribution as well as of the front location. Table 1 numerically presents the comparison of the methods. The front tracking method had the maximum temperature error more than 10^3-times smaller than the interface capturing methods. A similar conclusion can be drawn for the mean temperature error. The maximum temperature errors of the front capturing methods shown in Table 1 are at least 10-times higher than ΔT, and therefore they cannot be caused by the considered non-isothermal phase change. As for the front location, absolute and relative errors are presented in Table 1. Figure 10 shows the exact and simulated front positions. The relative error of the front location is about 0.02% in case of

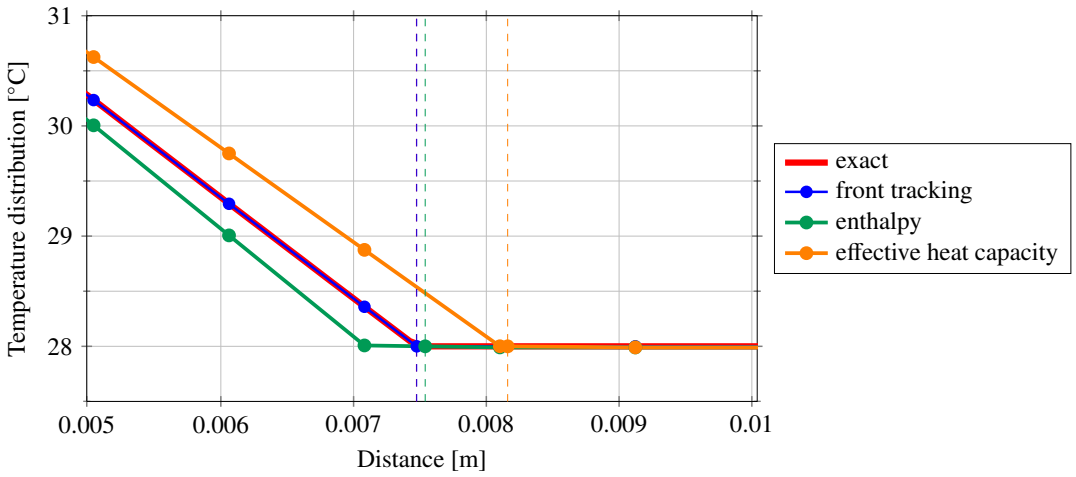

Figure 9. Detail of exact and simulated temperature distributions near the front location at time $t = 1$ hr.

the front tracking method while about 1% in case of the enthalpy method and even about 9% for the effective heat capacity method. The effective heat capacity method provides the worst results mainly due to the very narrow temperature interval of the phase change in which the heat capacity steeply increases and decreases. The enthalpy method is more robust from this point of view as the enthalpy only increases (is monotonic) with the temperature.

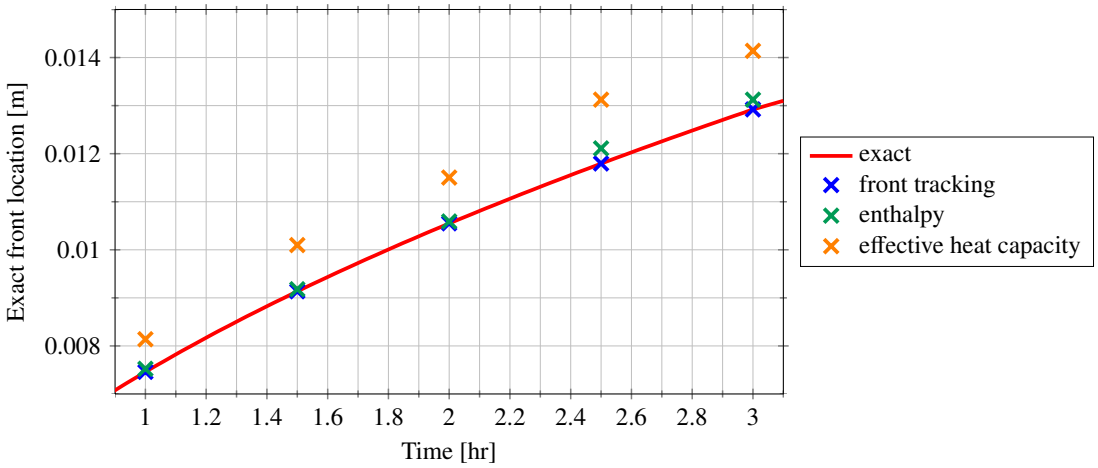

Figure 10. Comparison of the exact and simulated front locations in time.

5. Conclusion

The Stefan melting problem in a half space was investigated by means of interface tracking and interface capturing methods. The analysis shows that the front tracking method achieves very precise simulation results in comparison to the enthalpy and the effective heat capacity methods. The numerical accuracy (the error in the temperature distribution and the front location) of the front tracking algorithm is of 10^3-times higher order than in case of the interface capturing methods.

Acknowledgments

This work was supported by the Czech Science Foundation under the contract GA15-11977S.

References

[1] Osterman E, Butala V and Stritih U 2015 *Energy Build.* **106** 125–33
[2] Laing D, Bahl C, Bauer T, Lehmann D and Steinmann W D 2011 *Sol. Energy* **85** 627–33
[3] Mosaffa A H and Farshi L G 2016 *Appl. Energy* **162** 515–26
[4] Odunsi A, O'Donova T S, Reay D A 2016 *Appl. Therm. Eng.* **93** 1377–93
[5] Liu S, Li Y and Zhang Y (2014) *Renew. Sust. Energ. Rev.* **33** 659–74
[6] Voller V R and Swaminathan C R 1990 *Int. J. Numer. Methods Eng.* **30** 875–98
[7] Bonacina C, Gomini G 1973 *Int. J. Heat Mass Transf.* **16** 1825–32
[8] Shyy W, Udaykumar H S, Rao M M, Smith R W 1996 *Computational Fluid Dynamics with Moving Boundaries* (Philadelphia: Taylor and Francis)
[9] Udaykumar H S, Shyy W, Rao M 1996 *Int. J. Numer. Methods Fluids* **22** 691–712
[10] Li C Y, Garimela S V and Simpson J E 2003 *Numer. Heat Tranf. B-Fundam.* **43** 117-41
[11] Browne D J and Hunt J D 2004 *Numer Heat Tranf. B-Fundam.* **45** 395–419
[12] Seredynski M, Lapka P, Banaszek J, Furmanski P 2015 *Int. J. Heat Mass Transf.* **90** 790–9
[13] McFadden S and Browne D J 2012 *Appl. Math. Model.* **33** 1397–416
[14] Banaszek J and Seredynski M 2012 *Int. J. Heat Mass Transf.* **55** 4334–9
[15] Hahn D W and Özişik 2012 *Heat Conduction* (New York: Wiley)
[16] *Rubitherm RT 28 HC specification list* available online at `www.rubitherm.de` under Products, Organic PCM